Solar Sail Heliocentric Earth-Following Orbits

Jeannette Heiligers[1] and Colin R. McInnes[2]

University of Strathclyde, Glasgow, G1 1XJ

I. Introduction

Solar sail technology development is rapidly gaining momentum after recent successes such as JAXA's IKAROS mission [1] and NASA's NanoSail-D2 mission [2]. Research in the field is flourishing and new solar sail initiatives, such as NASA's Sunjammer mission, are scheduled for the future [3]. Solar sails exploit the radiation pressure generated by solar photons reflecting off a large, highly reflecting sail to produce a continuous thrust force. They are therefore not constrained by propellant mass [4], which gives them huge potential for long-lifetime and high-energy mission concepts and enables a range of novel applications. One such family of applications are non-Keplerian orbits (NKOs) [5, 6], where the force due to solar radiation pressure on a solar sail is used to displace an orbit away from a natural Keplerian orbit. Different types of NKOs exist, including NKOs in the two-body problem (either Sun-centered or Earth-centered) and NKOs in the well-known circular restricted three-body problem (CR3BP). In the Sun-centered two-body problem, NKOs are determined by considering the solar sail spacecraft dynamics in a rotating frame of reference. By setting the time derivatives of the position vector equal to zero, equilibrium solutions are found in the rotating frame that correspond to displaced circular orbits in an inertial frame. Such Sun-centred NKOs allow a spacecraft to be synchronous with a planet at any heliocentric distance inward from the target planet and/or to displace a solar sail spacecraft out of the ecliptic plane for solar polar observations,

[1] Research Associate, Advanced Space Concepts Laboratory, Department of Mechanical and Aerospace Engineering, James Weir Building, 75 Montrose Street, Glasgow, G1 1XJ, UK, jeannette.heiligers@strath.ac.uk.

[2] Director, Advanced Space Concepts Laboratory, Department of Mechanical and Aerospace Engineering, James Weir Building, 75 Montrose Street, Glasgow, G1 1XJ, UK, colin.mcinnes@strath.ac.uk.

interplanetary communication, and astronomical observations [7]. A similar approach can be used to find solar sail NKOs in the Earth two-body problem, creating, for example, orbits on the Earth's nightside to study its magnetotail and interaction with the solar wind [8] and displaced geostationary orbits to create additional geostationary slots for telecommunication, Earth observation, and weather satellites [9, 10]. Finally, in the CR3BP, solar sails have been demonstrated to extend the five Lagrange points to a continuum of new artificial equilibrium points (AEPs) [11] and can be used to create periodic orbits around these AEPs [12]. The applications of these NKOs are abundant, including one-year periodic orbits high above the ecliptic in the Sun-Earth system for polar observations [12], solar sail trajectories above the Earth-Moon L_2 point to establish an Earth-Moon communication link [13] and solar sail Halo orbits sunward of the Sun-Earth L_1 point to increase the warning times for solar storms [14, 15].

Rather than displacing the orbit, the force due to solar radiation pressure on a solar sail can also be used to create an artificially precessing NKO. For example, the GeoSail mission [16] proposed the use of a solar sail to rotate an elliptic geocentric orbit in the ecliptic plane such that apogee remains on the night side of the Earth to enable continuous observations of the geomagnetic tail. In this technical note, the concept of rotating an elliptic orbit by means of a solar sail is considered further by investigating precessing, heliocentric, and Earth-following orbits. The sail orbit's aphelion follows the Earth's orbital motion throughout the year and is always directed along the Sun-Earth line, allowing extended observations for space weather forecasting and Near Earth Objects (NEOs) surveillance activities.

II. Orbit definition

The concept of heliocentric Earth-following orbits is illustrated in Figure 1: a solar sail acceleration is used to rotate the line of apsides of an elliptic heliocentric orbit such that aphelion follows the Sun-Earth line. The sail contributes an acceleration, $\mathbf{f}$, to the spacecraft trajectory based on the vehicle's location with respect to the Sun. Since a planar case is considered (such that the solar sail spacecraft orbits the Sun in the ecliptic plane), the evolution of the osculating orbital elements and time is given by the following four Lagrange equations [17]:

$$\frac{da}{d\theta} = \frac{2pr^2}{\mu_S\left(1-e^2\right)^2}\left(e\sin\theta\, f_r + \frac{p}{r}\, f_t\right) \tag{1}$$

$$\frac{de}{d\theta} = \frac{r^2}{\mu_S}\left(\sin\theta f_r + \left(1+\frac{r}{p}\right)\cos\theta f_t + e\frac{r}{p} f_t \right) \tag{2}$$

$$\frac{d\omega}{d\theta} = \frac{r^2}{\mu_S e}\left(-\cos\theta f_r + \left(1+\frac{r}{p}\right)\sin\theta f_t \right) \tag{3}$$

$$\frac{dt}{d\theta} = \frac{r^2}{\sqrt{\mu_S p}}\left(1-\frac{r^2}{\mu_S e}\left(\cos\theta f_r - \left(1+\frac{r}{p}\right)\sin\theta f_t\right)\right) \tag{4}$$

with a the semi-major axis, e the eccentricity, ω the argument of periapsis, θ the true anomaly, $\mu_S = 1.3272\times10^{11}$ kg^3/s^2 the gravitational parameter of the Sun, $p = a\left(1-e^2\right)$, $r = p/\left(1+e\cos\theta\right)$, and f_r and f_t the radial and transverse components of the perturbing solar sail acceleration.

By definition, a heliocentric Earth-following orbit has to satisfy the following conditions:

$$\begin{gathered} a_0 = a_f \\ e_0 = e_f \\ \Delta\omega = \Delta t\frac{2\pi}{P} = \left(t_f - t_0\right)n_E,\ \Delta t = \left(t_f - t_0\right) \end{gathered} \tag{5}$$

where the subscripts '0' and 'f' indicate the conditions at $\theta = 0$ and $\theta = 2\pi$, P the Earth's orbital period and n_E is the Earth's mean motion. The semi-major axis and eccentricity must thus remain unchanged over one orbital revolution and the argument of perihelion needs to increase by an amount equal to the angular distance that the Earth traverses in time Δt. Here, Δt is the spacecraft orbital period (accounting for changes in the orbit period due to the perturbing solar sail acceleration, see Eq. (4)). Note that the Earth's orbit is assumed to be circular.

The conditions in Eq. (5), i.e., no change in the semi-major axis and eccentricity and only a change in the argument of perihelion, are satisfied by choosing a simple apsides steering law. An apsides steering law creates an acceleration opposite to the eccentricity vector, i.e., parallel to the (instantaneous) line of apsides and directed towards aphelion, as shown in Figure 1.

The radial and transverse components of the acceleration are then defined by:

$$\mathbf{f} = \begin{pmatrix} f_r \\ f_t \end{pmatrix} = f\begin{pmatrix} \cos\left(\pi-\theta\right) \\ \sin\left(\pi-\theta\right) \end{pmatrix} = f\begin{pmatrix} -\cos\theta \\ \sin\theta \end{pmatrix} \tag{6}$$

with

$$f = \beta \frac{\mu_S}{r^2} \left(\hat{\mathbf{r}} \cdot \hat{\mathbf{n}} \right)^2 = \beta \frac{\mu_S}{r^2} \cos^2 \theta \tag{7}$$

Equation (7) is based on an ideal solar sail model, which assumes pure specular reflection of the impinging photons. The solar sail acceleration vector then acts perpendicular to the solar sail surface, i.e., in direction $\hat{\mathbf{n}}$. The parameter β is the solar sail lightness number, which is the ratio of the solar radiation pressure acceleration and the solar gravitational acceleration. Or, equivalently, β can be expressed as a function of the sail area to spacecraft mass ratio, σ, and the critical solar sail loading parameter, $\sigma^* = 1.53$ g/m^2 [4]:

$$\beta = \frac{\sigma^*}{\sigma} \tag{8}$$

As a realistic near-term value for the lightness number, the Sunjammer mission is taken as a reference. Sunjammer is a NASA solar sail technology demonstration mission that is scheduled for launch post-2015 and targets a sub-L_1 point [3]. With a solar sail area of approximately 1200 m^2 and a mass of 45 kg, the lightness number of the Sunjammer sail is assumed to be in the range 0.0388-0.0455 [18] and is used throughout this paper to assess the near-term performance of the proposed concepts. The extremes of this range are indicated by $\beta_{SJ,\min}$ and $\beta_{SJ,\max}$, respectively.

A limitation of solar sails is their inability to generate an acceleration component in the direction of the Sun [4]. The steering law described in Eq. (6) therefore cannot be maintained when $0 \le \theta < \frac{1}{2}\pi$ or $\frac{3}{2}\pi < \theta \le 2\pi$. Within these ranges, the attitude of the sail is assumed to be turned edgewise to the Sun, thus the sail does not contribute an additional acceleration.

Substituting the adopted steering laws into Eqs. (1)-(4) gives:

$$\left.\begin{aligned} \frac{da}{d\theta} &= \frac{2a}{1-e^2} \beta \cos^2 \theta \sin \theta \\ \frac{de}{d\theta} &= \beta \frac{\cos^3 \theta \sin \theta + e \cos^2 \theta \sin \theta}{1 + e \cos \theta} \\ \frac{d\omega}{d\theta} &= \beta \frac{1}{e} \cos^2 \theta \left(1 + \frac{\sin^2 \theta}{1 + e \cos \theta} \right) \\ \frac{dt}{d\theta} &= \frac{r^2}{\sqrt{\mu_S p}} \left(1 + \beta \frac{1}{e} \cos^2 \theta \left(1 + \frac{\sin^2 \theta}{1 + e \cos \theta} \right) \right) \end{aligned}\right\} \quad \frac{1}{2}\pi \le \theta \le \frac{3}{2}\pi \qquad \left.\begin{aligned} \frac{da}{d\theta} &= 0 \\ \frac{de}{d\theta} &= 0 \\ \frac{d\omega}{d\theta} &= 0 \\ \frac{dt}{d\theta} &= \frac{r^2}{\sqrt{\mu_S p}} \end{aligned}\right\} \quad \begin{aligned} &0 \le \theta < \frac{1}{2}\pi \\ &\frac{3}{2}\pi < \theta \le 2\pi \end{aligned} \tag{9}$$

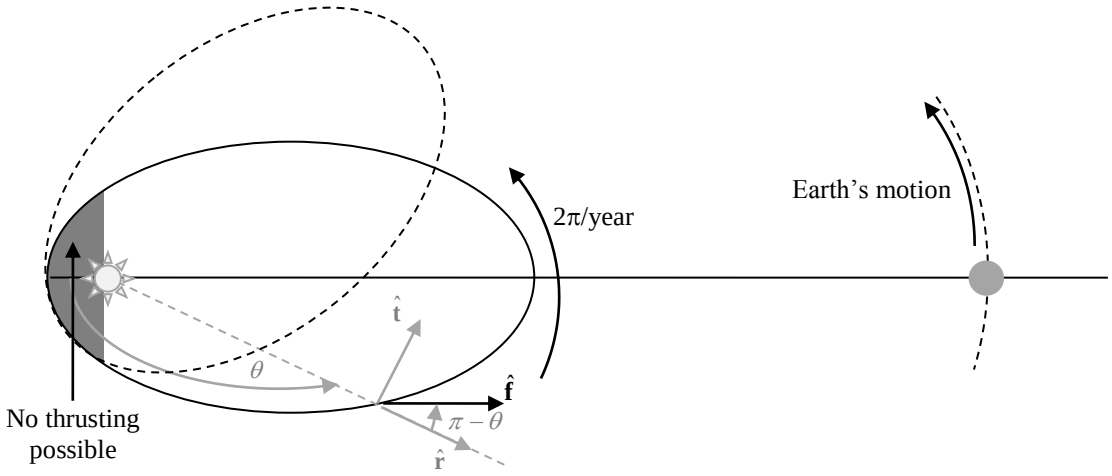

Figure 1. Illustration of heliocentric Earth-following orbits.

III. Time invariant semi-major axis and eccentricity

A first assessment of the heliocentric Earth-following orbits can be made by assuming that the semi-major axis and eccentricity do not change during the orbital motion (referred to as the 'constant a and e' case). Section IV will consider the actual variation in these orbital elements (referred to as the 'time-varying a and e' case). When keeping a and e constant over one revolution, the equations for the argument of perihelion and time in Eq. 9 can be integrated analytically over the time domains specified to obtain the change in these variables after one orbital revolution:

$$\Delta\omega = \frac{\beta}{6e^5}\left(-4e\left(e^2-3\right)+3\pi\left(e^4-e^2+2\right)-12\pi\left(e+1\right)\sqrt{\frac{2}{e+1}-1}+12\sqrt{-e^2+1}\tan^{-1}\left(\frac{\sqrt{-e^2+1}}{e}\right)\right) \tag{10}$$

$$\Delta t = 2\pi\sqrt{\frac{a^3}{\mu_S}}+\frac{a^2}{e^5\sqrt{a\mu_S}}\left(\beta\left(\left(-\pi e^4-3e^3-2\pi e^2+6e+3\pi\right)\sqrt{-e^2+1}+\left(2e^4+7e^2-6\right)\pi\right)-\right.$$
$$\left.-2\beta\left(2e^4+7e^2-6\right)\sin^{-1}\left(\sqrt{\frac{-e+1}{2}}\right)\right) \tag{11}$$

From Eq. (11) the Keplerian orbital period (first term on the right hand side) and the deviation from this period due to the sail's contribution is clear. By substituting Eqs. (10) and (11) into the third equation of Eq. (5), the lightness number required to maintain a heliocentric Earth-following orbit can be obtained as:

$$\beta = \frac{2a^2e^5n_E\pi}{\left(a^2n_E\left(\left(2e^4+7e^2-6\right)\left(2\sin^{-1}\left(\sqrt{\frac{-e+1}{2}}\right)-\pi\right)-\left(-\pi e^4-3e^3-2\pi e^2+6e+3\pi\right)\sqrt{-e^2+1}\right)-\right.} \quad (12)$$
$$\left.\frac{\sqrt{a\mu_S}}{6}\left(4e\left(e^2-3\right)-3\pi\left(e^4-e^2+2\right)+12\left(e+1\right)\pi\sqrt{\frac{2}{e+1}-1}-12\sqrt{-e^2+1}\tan^{-1}\left(\frac{\sqrt{-e^2+1}}{e}\right)\right)\right)$$

Since β is a function of the semi-major axis and eccentricity only, contours of equal lightness number can be drawn as shown in Figure 2a (Figure 2b, which considers the time-varying a and e case is addressed in Section IV). The shaded areas indicate a minimum required perihelion of 0.25 AU due to limitations on the thermal tolerance of the sail film [4] and a maximum aphelion of 0.99 AU (i.e., the Sun-L_1-distance) to highlight the fact that the solution beyond that distance becomes less accurate due to the gravitational attraction of the Earth. Although the contours in Figure 2a extend up to large values for the lightness number, the validity of the results diminishes for such large sail accelerations since the Lagrange equations in Eqs. (1)-(4) only hold when the perturbing acceleration is small compared to the gravitational acceleration. From Eq. (7) it will be clear that this ratio of the solar sail acceleration to the gravitational acceleration is $\beta\left(\hat{\mathbf{r}}\cdot\hat{\mathbf{n}}\right)^2$ and therefore depends on the attitude of the sail with respect to the Sun-line. At the very maximum (when the sail faces the Sun), the ratio will equal to lightness number, but will on average be smaller, especially since the ratio is 0 for $0 \le \theta < \frac{1}{2}\pi$ or $\frac{3}{2}\pi < \theta \le 2\pi$. Therefore, for the lightness number of the Sunjammer sail, the Lagrange equations area ssumed to still hold. The contours for $\beta_{SJ,\min}$ and $\beta_{SJ,\max}$ are shown in Figure 3a from which it is clear that a Sunjammer sail would only enable heliocentric Earth-following orbits with small semi-major axes and small eccentricities. Note that Figure 3b, which considers the time-varying a and e case, is addressed in Section IV. To maximize the relative time spent along the Sun-Earth line, orbits with the maximum eccentricity (i.e., where the contours intersect the shaded area) are considered later on in this Note for further investigation. The orbital parameters of these orbits are given in Table 1, while a corresponding plot of the orbit when $\beta = \beta_{SJ,\min}$ appears in Figure 4a using an inertial reference frame where the

$x-$axis points towards the Earth at time $t=0$ or equivalently at $\theta=0$. From Figure 4b (where time is made dimensionless such that 1 year equals 2π), it is clear that the third condition in Eq. (5) is satisfied.

a) b)

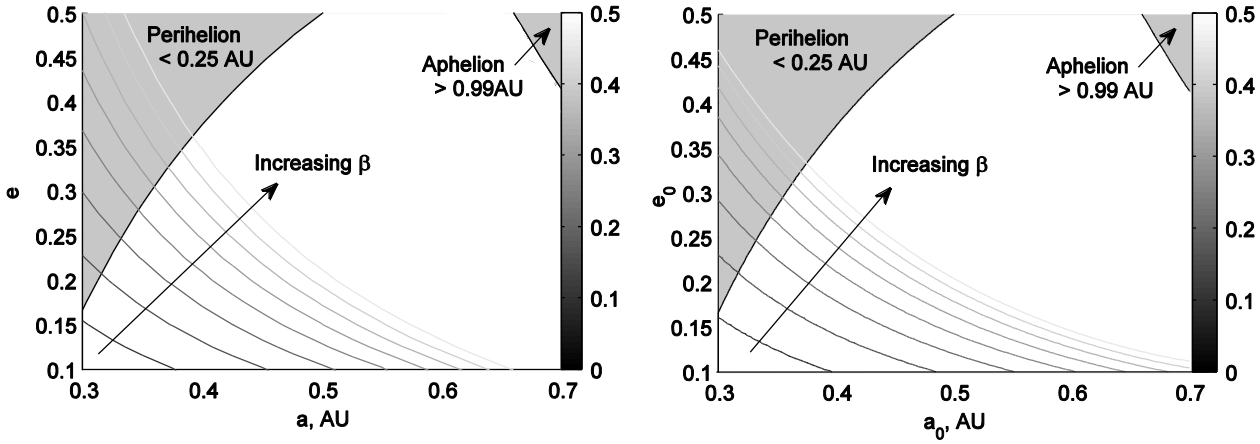

Figure 2. Contours of equal lightness number for β = [0.1 0.15 0.2 0.25 0.3 0.35 0.4 0.45] for heliocentric Earth-following orbits. a) Constant *a* and *e*. b) Time-varying *a* and *e*.

a) b)

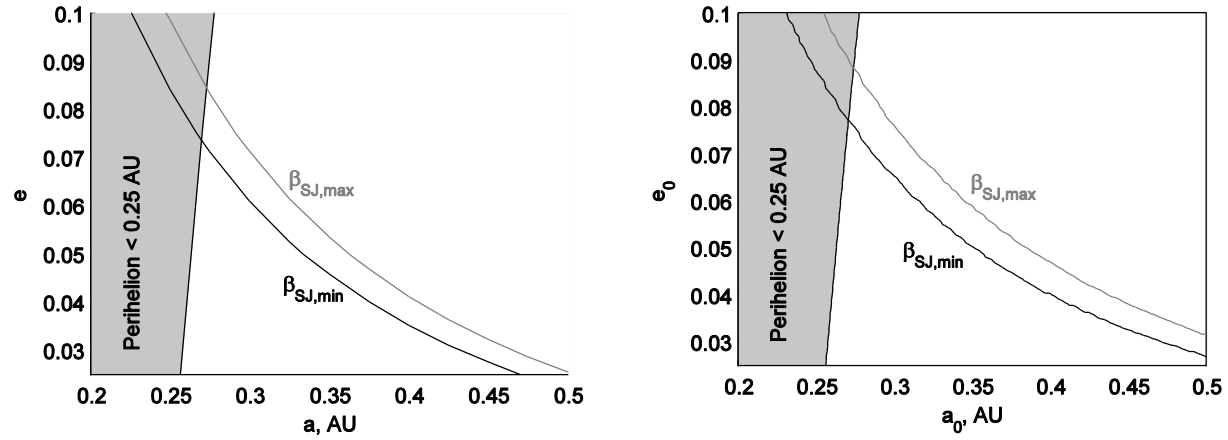

Figure 3. Contours of equal lightness number for β = [0.0388 0.0455] for heliocentric Earth-following orbits. a) Constant *a* and *e*. b) Time-varying *a* and *e*.

Table 1. Semi-major axis and eccentricity of selected heliocentric Earth-following orbits.

		Constant a and e	Time-varying a and e
$\beta = \beta_{SJ,\min}$	a_0, AU	0.2698	0.2708
	e_0	0.0736	0.0777
	Period, days	60.8	61.8
$\beta = \beta_{SJ,\max}$	a_0, AU	0.2728	0.2742
	e_0	0.0847	0.0888
	Period, days	62.1	63.5

a) b)

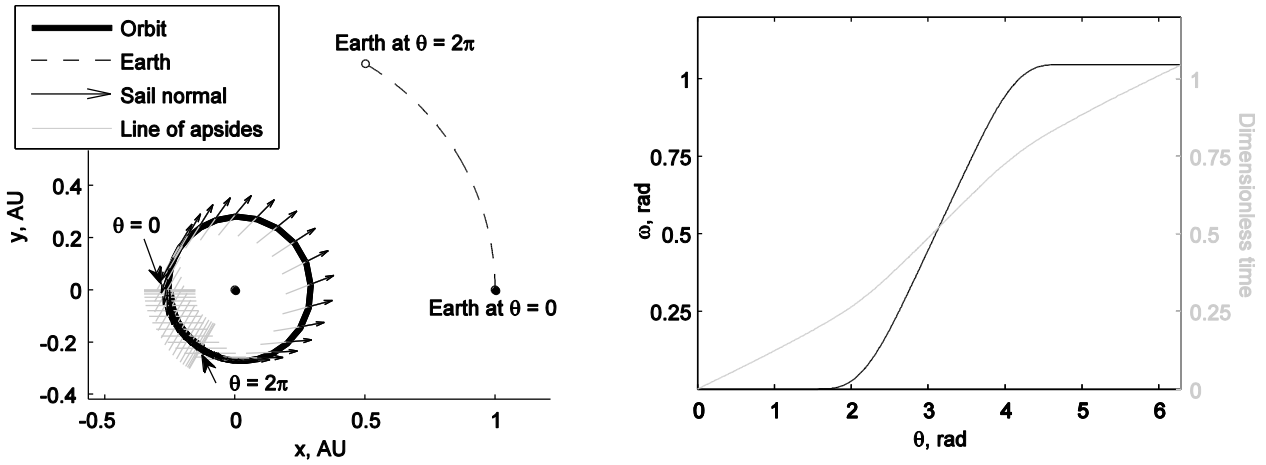

Figure 4. Heliocentric Earth-following orbits with constant a = 0.2698 AU and e = 0.0736 for $\beta = \beta_{SJ,\min}$. a) Orbital evolution. b) Evolution of argument of perihelion and dimensionless time.

IV. Time variant semi-major axis and eccentricity

The assumption of constant semi-major axis and eccentricity in the previous section allows an analytical investigation into the heliocentric Earth-following orbits. Removing this assumption and taking the actual variation of a and e into account will have an effect on the performance of the solar sail. A numerical approach for integrating Eq. (9) is adopted: a fine mesh in the initial value for a and e at the orbit perihelion is considered (i.e., a_0 and e_0) and for each combination the equations of motion are integrated for a range of β - values. For each value for β, the third condition in Eq. (5) is evaluated and the value that matches the condition closest is considered

the required lightness number. The results appear in Figure 2b, which clearly shows a difference with the results in Figure 2a that assumed constant a and e along the orbit. Interestingly, for small values of the lightness number, the performance is improved. This improvement is also clear from the contours for $\beta_{SJ,\min}$ and $\beta_{SJ,\max}$ in Figure 3b; the intersection between the contours and the shaded area occurs at larger values for the semi-major axis and eccentricity, which implies that the spacecraft will linger longer along the Sun-Earth line along a larger, more elliptical – and desirable - orbit. The orbital elements of these orbits are included in Table 1, while further details of the time dependencies of the orbital elements are provided in Figure 5 for $\beta = \beta_{SJ,\min}$ where the results of Section III for constant semi-major axis and eccentricity are included as dashed lines for comparison purposes.

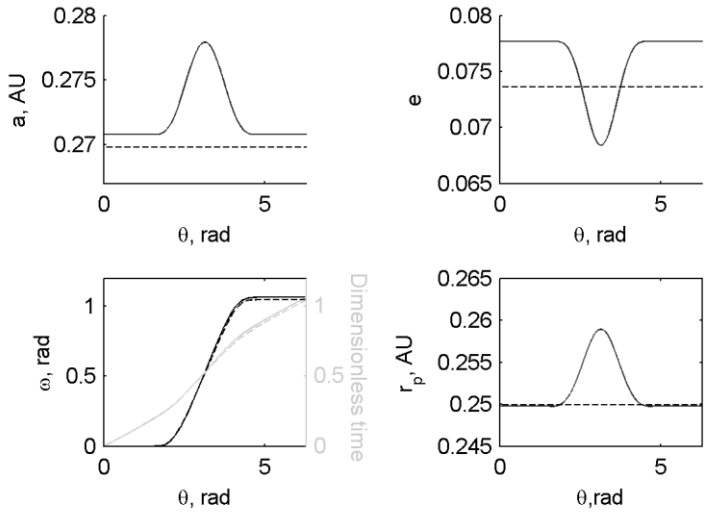

Figure 5. Evolution of Keplerian elements for heliocentric Earth-following orbits for $\beta = \beta_{SJ,\min}$. Solid lines are for time-varying a and e (a_0 = 0.2708 AU and e_0 = 0.0777), while dashed lines are for constant a = 0.2698 AU and e = 0.0736. The bottom right plot shows the evolution of the perihelion radius, r_p.

V. Optimal steering law

Although the apsides steering law of the previous section allows for a simple steering of the solar sail, it may not be optimal for extended observations along the Sun-Earth line as will be discussed in Section VI. Therefore, this section investigates the optimal steering law to maximize the time spent near or along the Sun-Earth line or equivalently to maximize the mean eccentricity of the orbit. This optimal steering law is found by solving the

accompanying optimal control problem using a particular implementation of a direct pseudospectral method in C++ known as PSOPT [19]. A condensed definition of the optimal control problem is given below.

The objective, J, is defined as:

$$J = -\int_{\theta=0}^{\theta=\theta_f} e(\theta)^2 \, d\theta \tag{13}$$

The states, $\mathbf{x}(t)$, and controls, $\mathbf{u}(t)$, as well as bounds on these variables are defined as:

$$\begin{bmatrix} 0.2 \text{ AU} & 0 & 0 & 0 \end{bmatrix}^T \le \mathbf{x}(t) = \begin{bmatrix} a & e & \omega & t \end{bmatrix}^T \le \begin{bmatrix} \text{AU} & 0.99 & 2\pi & 4\pi \end{bmatrix}^T \tag{14}$$

$$\begin{bmatrix} 0 & -1 \end{bmatrix}^T \le \mathbf{u}(t) = \begin{bmatrix} n_r & n_t \end{bmatrix}^T \le \begin{bmatrix} 1 & 1 \end{bmatrix}^T \tag{15}$$

Note the lower limit on the radial control component, which takes into account the inability of a solar sail to generate an acceleration component in the direction of the Sun.

The dynamics are defined in Eqs. (1)-(4) and the event constraints are the required conditions defined for heliocentric Earth-following orbits in Eq. (5) as well as $\omega_0 = t_0 = 0$. Finally, two path constraints are included to ensure that the norm of the control vector is unity and that perihelion is always larger than 0.25 AU:

$$\begin{aligned} |\mathbf{u}(t)| &= 1 \\ a(1-e) &\ge 0.25 \text{ AU} \end{aligned} \tag{16}$$

The intial guess to initialise the optimal control problem is taken equal to the heliocentric Earth-following orbit found in the previous section, i.e., with time-varying semi-major axis and eccentricity, and with an apsides steering law. Figure 6 shows the results for $\beta = \beta_{SJ,\min}$ with plot a providing the eccentricity profile that provides the maximum mean eccentricity. Plots b and c clearly show the difference between the apsides steering law and the optimal steering law: thrusting extends beyond the feasible domain for apsides steering, i.e., beyond $\frac{1}{2}\pi \le \theta \le \frac{3}{2}\pi$, while still satisfying the constraint that the sail cannot generate an acceleration in the direction of the Sun, and is directed more radially than the apsides steering law.

VI. Surveillance zone analysis

The amount of time spent by the spacecraft in a particular "surveillance zone" is considered in this section to assess the performance of heliocentric Earth-following orbits for extended observations along the Sun-Earth line.

This surveillance zone is defined through the angle $\varepsilon_{\lim}$, which is measured from the Sun-Earth line (see Figure 7a). To compare the performance of the heliocentric Earth-following orbits, the observation time achieved with a Keplerian orbit – equal in size as the optimal heliocentric Earth-following orbit - is also considered. Because Keplerian orbits are inertially fixed, aphelion will only be aligned once per synodic period of the Earth-spacecraft system. At other times, the Earth and aphelion may be in opposition with respect to the Sun, losing out on valuable observation time.

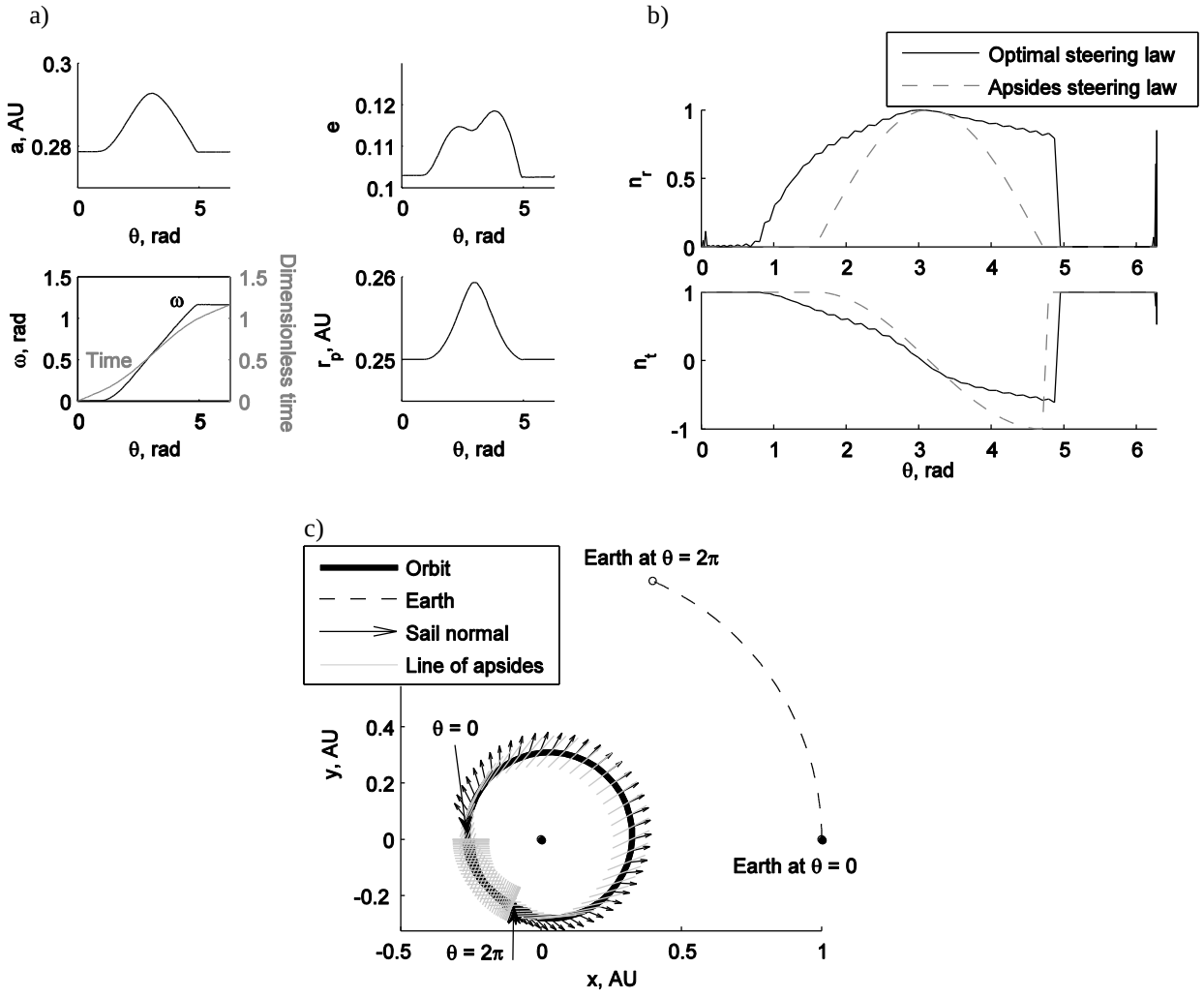

Figure 6. Optimal heliocentric Earth-following orbit for $\beta = \beta_{SJ,\min}$. a) Evolution of Keplerian elements with r_p the perihelion radius. b) Optimal steering law. c) Orbit evolution.

For both the heliocentric Earth-following orbit as well as for the Keplerian reference orbit, the time spent within the surveillance zone depends on the initial orientation of the orbit with respect to the Sun-Earth line. This orientation is given by the initial value of the argument of perihelion, which is measured from the Sun-Earth line at time $t = 0$. To properly phase heliocentric Earth-following orbits, the optimal initial orientation is $\omega_0 = \pi$. This property is clear from the bottom left plot in Figure 5 and Figure 6a, which show the symmetry in the orbit's evolution and the fact that aphelion is located at the instantaneous Sun-Earth line (i.e., the intersection of the two curves at $\theta = \pi$). For the Keplerian orbit, the maximum observation time in the first orbital revolution is obtained when, again, aphelion coincides with the instantaneous Sun-Earth line, see Figure 7b. Since the orbit is inertially fixed, this means that ω_0 can be derived from the angular distance the Earth traverses in half the Keplerian orbital period. Using time in its dimensionless form, the argument of perihelion for the Keplerian reference orbit, ω_K, can thus be derived from:

$$\omega_K = \pi + \Delta t = \pi + \Delta t_{s/c} = \pi + \tfrac{1}{2} P_{\text{orbit}} \tag{17}$$

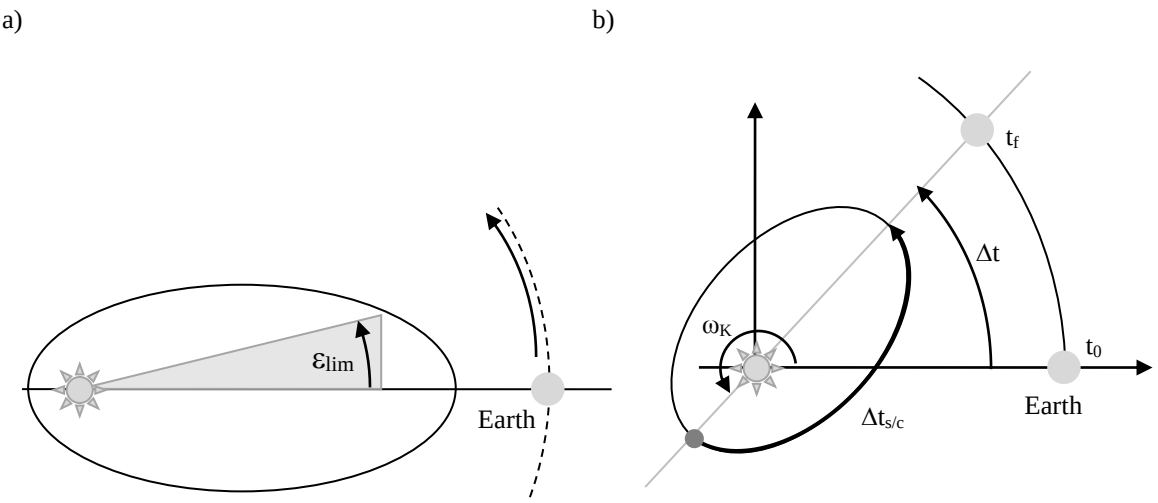

Figure 7. a) Definition of the surveillance zone. b) Orbital geometry for Keplerian reference orbit.

The results of the surveillance zone analysis are provided in Figure 8, Figure 9, and Table 2 for both $\beta_{SJ,\min}$ and $\beta_{SJ,\max}$, for the Keplerian orbit (open markers and lower light-grey line), the apsides steering law (solid markers and middle black line), and optimal control laws (crosses and upper grey line) and for three different values of $\varepsilon_{\lim}$: 10, 20, and 45 degrees. From the observation time per orbit (Figure 8a and Figure9a) it is immediately clear that the heliocentric Earth-following orbits enable a constant number of days per orbit for useful observation because the Earth-sail configuration is the same in each orbital revolution. Also, the Keplerian reference orbit enables an adequate coverage during the first orbital revolution, but because it is inertially fixed, the observation time is reduced in subsequent orbits. Consequently, a smaller overall percentage observation time for Keplerian orbits is available compared to the heliocentric Earth-following orbits (see Figure 8b, Figure 9b, and Table 2). For example, for $\beta = \beta_{SJ,\min}$ and $\varepsilon_{\lim} = 45^{\circ}$, the overall percentages are 25.6 percent (Keplerian), 29.3 percent (apsides steering law), and 32.2 percent (optimal steering law). This means that the heliocentric Earth-following orbits allow 3.7 percent (apsides steering law) and 6.6 percent (optimal steering law) more observation time, or, equivalently, increase the percentage observation time by a factor 1.14 and 1.26 compared to a Keplerian orbit. When inspecting the other results in Table 2 it appears that very similar factors hold for all other cases, i.e., for $\beta = \beta_{SJ,\min}$, $\beta = \beta_{SJ,\max}$, and for each value for $\varepsilon_{\lim}$. However, when building on the technology developed for Sunjammer and assuming larger values for the lightness number, e.g. $\beta = 0.1$, the apsides and optimal steering laws can increase the percentage observation time compared to a Keplerian orbit by a factor 1.42 and 1.79, respectively. These improvements underpin the potential of the heliocentric Earth-following orbits for the applications outlined in the following section.

VII. Applications

Two particular applications are envisaged for heliocentric Earth-following orbits: space weather forecasting [20] and Near Earth Objects (NEOs) surveillance [21]. Both require continuous observation along the Sun-Earth line, which can be achieved in an efficient way by the heliocentric Earth-following orbits if multiple spacecraft are phased along the orbit.

For space weather forecasting purposes, the solar coronal mass ejections that travel from the Sun-Earth line must be detected in order to warn operators of ground and space assets of incoming space weather events. These events can have detrimental effects such as power outages, damage to oil pipelines, need for aviation re-routing, damage to Earth-orbiting satellites, and hazardous conditions for astronauts onboard the International Space Station. Measurements taken by spacecraft located in a Halo orbit around the classical L_1 point (SOHO (ESA/NASA, 1996), ACE (NASA, 1997), and WIND (NASA, 2004)) are currently used to generate these warnings [22]. However, because of their relatively close distance to the Earth, warning times from these satellites are only 30-60 minutes. Previous and current proposals to use a solar sail to be stationed along the Sun-Earth line sunward of the classical L_1 point, the sub-L_1 concept, would result in an approximate increase in this warning time of a factor 2 [14, 15]. With a very small aphelion distance of 0.3229 AU along the Sun-Earth line this increase in warning time could be further extended to a factor 68 by the optimal heliocentric Earth-following orbits, keeping in mind that these would require a constellation of solar sail spacecraft while the sub-L_1 concept could be achieved with a single satellite.

Concerning the NEOs surveillance application, the heliocentric Earth-following orbits provide a means to detect NEOs that orbit the Sun within Earth's orbit or more specifically objects that approach the Earth from the direction of the Sun. These pose an increased danger to the Earth since they cannot be tracked from ground-based optical telescopes due to solar radiation disturbances [23]. By orbiting far within Earth's orbit, the heliocentric Earth-following orbits provide a way to track these objects, increasing the portion of the sky that can be surveiled compared to ground-based measurements. This is demonstrated in Figure 10, which provides contours of the minimum asteroid size detectable from either ground-based observations (in the white area) and additional observations from aphelion of the optimal heliocentric Earth-following orbits for $\beta = \beta_{SJ,\min}$ (in the light grey area). To compute the values in Figure 10, the approach described in References [23, 24] is adopted (with a limiting visual magnitude of 24 and 23 for ground based and space-based observations, respectively). For observations from the heliocentric Earth-following orbits only the contours in the grey are shown, which represents the 40 deg Solar Exclusion Zone (SEZ) in which asteroids cannot be detected from Earth. A similar SEZ exists for observations from aphelion, which is represented by the dark grey area. The figure clearly shows that the heliocentric Earth-following orbits can significantly extend the portion of the solar system that can be surveyed for asteroids compared to ground-

based observations. Furthermore, when extending the contours into the white area, some improvements in minimum asteroids size are possible compared to ground-based observations (e.g. the 75 m contour for the heliocentric Earth-following case will intersect with the 100 m contour for ground-based observations). Again, it should be noted that these results are only feasible from aphelion of the heliocentric Earth-following orbits and therefore a constellation of spacecraft will be required to maintain such a performance over time.

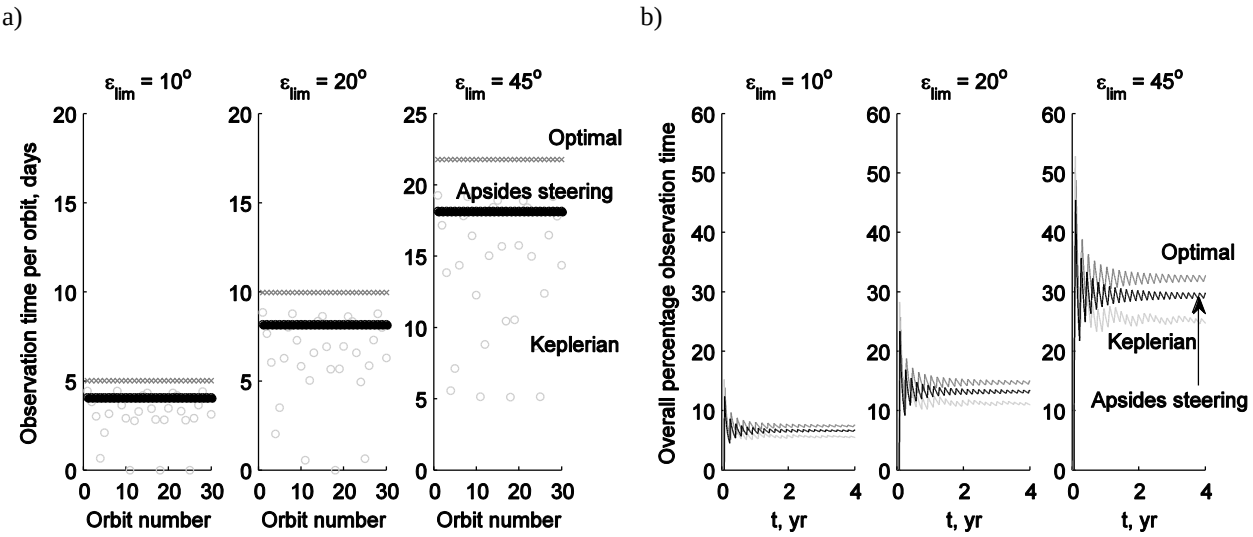

Figure 8. Surveillance zone analysis for $\beta = \beta_{SJ,\min}$. a) Observation time per orbit. b) Observation time as percentage of elapsed time.

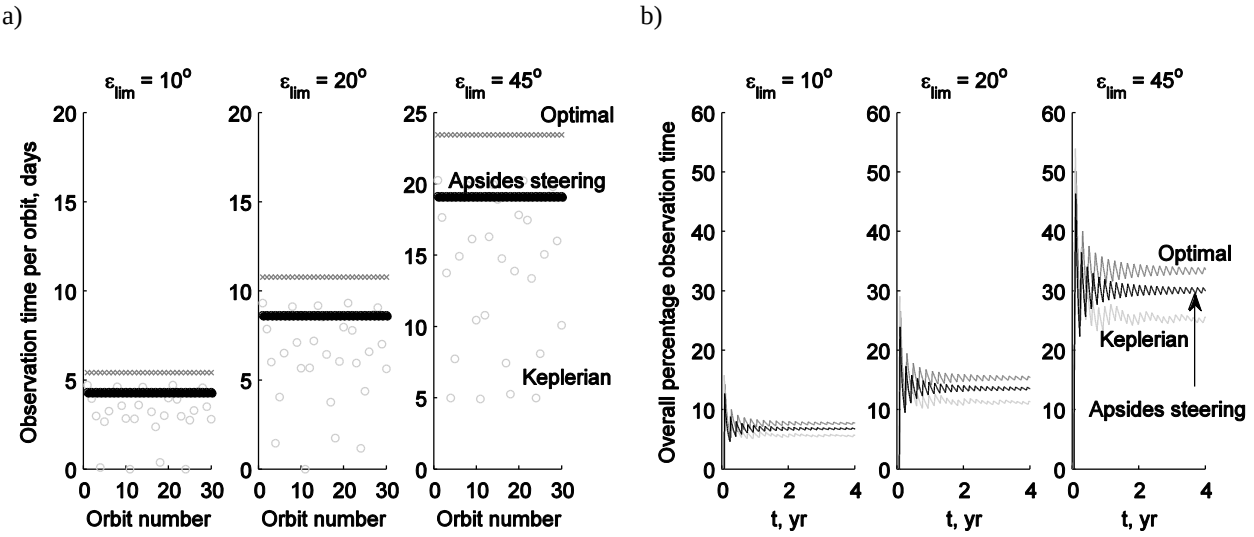

Figure 9. Surveillance zone analysis for $\beta = \beta_{SJ,\max}$. a-b) Observation time per orbit. c-d) Observation time as percentage of elapsed time.

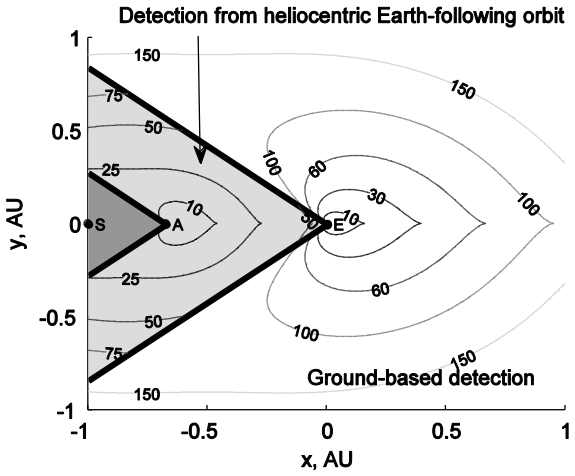

Figure 10. Minimum asteroid size (in meters) detectable represented in a Sun-Earth synodic reference frame. Contours in the white area are for ground-based detection; contours in the light grey area (i.e. in the 40 deg Solar Exclusion Zone (SEZ) from Earth) are for additional detection from aphelion of the optimal heliocentric Earth-following orbit for $\beta = \beta_{SJ,\min}$. The dark grey area is the 40 deg SEZ for observations from aphelion. The labels S, A and E indicate the Sun, aphelion and Earth, respectively.

Table 2. Surveillance zone performance with t_{obs} the observation time per orbit and P the orbital period, both in days.

		$\varepsilon_{\lim}$		
		10°	20°	45°
$\beta_{SJ,\min}$	**Keplerian, $P = 53.7$**			
	Average t_{obs}	3.1	6.1	13.8
	Average $100 t_{obs}/P$	5.7	11.4	25.6
	Apsides thrusting, $P = 61.79$			
	t_{obs}	4.1	8.2	18.2
	$100 t_{obs}/P$	6.6	13.2	29.3
	Improvement factor compared to Keplerian	1.16	1.16	1.14
	Optimal thrusting, $P = 67.6$			
	t_{obs}	5.0	10.0	21.8
	$100 t_{obs}/P$	7.4	14.7	32.2
	Improvement factor compared to Keplerian	1.30	1.29	1.26
$\beta_{SJ,\max}$	**Keplerian, $P = 54.9$**			
	Average t_{obs}	3.1	6.3	14.0
	Average $100 t_{obs}/P$	5.7	11.4	25.4
	Apsides thrusting, $P = 63.5$			
	t_{obs}	4.3	8.6	19.1
	$100 t_{obs}/P$	6.8	13.6	30.1
	Improvement factor compared to Keplerian	1.19	1.19	1.19
	Optimal thrusting, $P = 70.3$			
	t_{obs}	5.4	10.8	23.4
	$100 t_{obs}/P$	7.7	15.3	33.4
	Improvement factor compared to Keplerian	1.35	1.34	1.32

VIII. Conclusions

This Note has introduced the concept of solar sail heliocentric Earth-following orbits. By exploiting the force due to solar radiation pressure on a solar sail, the line of apsides of a heliocentric orbit is rotated such that aphelion is always directed along the Sun-Earth line. This orbit control has been achieved with a simple apsides steering law. By further assuming that the semi-major axis and eccentricity remain constant along the orbit, an analytic expression for the required sail performance has been derived. Removing this assumption allows for slightly better performing

heliocentric Earth-following orbits for small sail lightness numbers. Compared to an inertially fixed Keplerian orbit, the heliocentric Earth-following orbits increase the time spent within a predefined cone around the Sun-Earth line by an average factor of 1.17 for a sail performance equal to that of NASA's Sunjammer mission (i.e., maximum sail lightness number of 0.0455). For an optimal solar sail steering law, which is directed more radially than the apsides steering law, this factor increases further to an average factor of 1.31. Further improvements in the performance can be achieved when considering a larger sail lightness number of 0.1 that should be achievable in the future by building upon the technology developed for Sunjammer. This lightness number can increase the percentage observation time compared to a Keplerian orbit by a factor 1.79. Applications of the heliocentric Earth-following orbits have been identified as space weather forecasting and NEOs surveillance, which both require continuous observations taken along the Sun-Earth line. This can be achieved by a phased constellation of solar sail satellites along the heliocentric Earth-following orbits.

Acknowledgments

This work was funded by the European Research Council Advanced Investigator Grant-227571, Visionary Space Systems: Orbital Dynamics at Extremes of Spacecraft Length-Scale.

References

1. Tsuda, Y., Mori, O., Funase, R., Sawada, H., Yamamoto, T., Saiki, T., Endo, T., and Kawaguchi, J. "Flight Status of IKAROS Deep Space Solar Sail Demonstrator," *Acta Astronautica* Vol. 69, No. 9-10, 2011, pp. 833-840. doi: 10.1016/j.actaastro.2011.06.005
2. Johnson, L., Whorton, M., Heaton, A., Pinson, R., Laue, G., and Adams, C. "NanoSail-D: A Solar Sail Demonstration Mission," *Acta Astronautica* Vol. 68, 2011, pp. 571-575. doi: 10.1016/j.actaastro.2010.02.008
3. L'Garde Inc. "L'Garde - Sunjammer." http://www.lgarde.com/programs/space-propulsion/sunjammer, Accessed 8 May 2013.
4. McInnes, C. R. *Solar Sailing: Technology, Dynamics and Mission Applications*. Berlin: Springer-Praxis Books in Astronautical Engineering, Springer-Verlag, 1999, pp. 1, 21, 40, 174.
5. McInnes, C. R. "Dynamics, Stability, and Control of Displaced Non-Keplerian Orbits," *Journal of Guidance, Control, and Dynamics* Vol. 21, No. 5, 1998, pp. 799-805. doi: 10.2514/2.4309
6. McInnes, C. R. "The Existence And Stability Of Families Of Displaced Two-Body Orbits," *Celestial Mechanics and Dynamical Astronomy* Vol. 67, No. 2, 1997, pp. 167-180. doi: 10.1023/A:1008280609889
7. McInnes, C., and Simmons, J. F. L. "Solar Sail Halo Orbits. Part I - Heliocentric Case," *Journal of Spacecraft and Rockets* Vol. 29, No. 4, 1992, pp. 466-471. doi: 10.2514/3.25487
8. McInnes, C. R., and Simmons, J. F. L. "Solar Sail Halo Orbit. Part II - Geocentric Case," *Journal of Spacecraft and Rockets* Vol. 29, No. 4, 1992, pp. 472-479.doi: 10.2514/3.55639
9. Baig, S., and McInnes, C. R. "Light-Levitated Geostationary Cylindrical Orbits Are Feasible," *Journal of Guidance, Control, and Dynamics* Vol. 33, No. 3, 2010, pp. 782-793. doi: 10.2514/1.46681
10. Heiligers, J., Ceriotti, M., McInnes, C. R., and Biggs, J. D. "Displaced Geostationary Orbit Design Using Hybrid Sail Propulsion," *Journal of Guidance, Control, and Dynamics* Vol. 34, No. 6, 2011, pp. 1852-1866. doi: 10.2514/1.53807

11. McInnes, C. R., McDonald, A. J., Simmons, J. F. L., and MacDonald, E. W. "Solar Sail Parking in Restricted Three-Body Systems," *Journal of Guidance, Control, and Dynamics* Vol. 17, No. 2, 1994, pp. 399-406. doi: 10.2514/3.21211
12. Waters, T. J., and McInnes, C. R. "Periodic Orbits Above the Ecliptic in the Solar-Sail Restricted Three-Body Problem," *Journal of Guidance, Control, and Dynamics* Vol. 30, No. 3, 2007, pp. 687-693. doi: 10.2514/1.26232
13. McInnes, C. R. "Solar Sail Trajectories at the Lunar L_2 Lagrange Point," *Journal of Spacecraft and Rockets* Vol. 30, No. 6, 1993, pp. 782-784. doi: 10.2514/3.26393
14. West, J. L. "The GeoStorm Warning Mission: Enhanced Opportunities Based on New Technology," *14th AAS/AIAA Spaceflight Mechanics Conference*. AAS-04-102, Maui, Hawaii, 2004.
15. Heiligers, J., Diedrich, B., Derbes, B., and McInnes, C. R. "Sunjammer: Preliminary End-to-End Mission Design," *2014 AIAA/AAS Astrodynamics Specialist Conference*. San Diego, CA, USA, 2014.
16. Macdonald, M., McInnes, C., Alexander, D., and Sandman, A. "GeoSail: Exploring the Magnetosphere Using a Low-cost Solar Sail," *Acta Astronautica* Vol. 59, 2006, pp. 757-767. doi: 10.1016/j.actaastro.2005.07.023
17. Fortescue, P., and Stark, J. *Spacecraft Systems Engineering*: Wiley, New York, 1995, pp. 94.
18. Heiligers, J., and McInnes, C. "Novel Solar Sail Mission Concepts for Space Weather Forecasting," *24th AAS/AIAA Space Flight Mechanics Meeting*. Santa Fe, NM, 2014.
19. Becerra, V. M. "Solving Complex Optimal Control Problems at No Cost with PSOPT," *IEEE Multi-conference on Systems and Control*. Yokohama, Japan, 2010.
20. Milan, S. "KuaFu: Exploring the Sun-Earth Connection," *Astronomy & Geophysics* Vol. 53, No. 4, 2012, pp. 4.21-4.24. doi: 10.1111/j.1468-4004.2012.53421.x
21. Perna, D., Barucci, M. A., and Fulchignoni, M. "The Near-Earth Objects and Their Potential Threat to Our Planet," *The Astronomy and Astrophysics Review* Vol. 21, No. 1, 2013, pp. 1-28. doi: 10.1007/s00159-013-0065-4
22. Stone, E. C., Frandsen, A. M., Mewaldt, R. A., Christian, E. R., Margolies, D., Ormes, J. F., and Snow, F. "The Advanced Composition Explorer.", *Space Science Reviews* Vol. 86, No. 1, 1998, pp. 1-22.
23. Stramacchia, M., Colombo, C., and Bernelli-Zazzera, F. "Distant Periodic Orbit for Space-Based Near Earth Objects Detection," *24th AAS/AIAA Space Flight Mechanics Meeting*. Santa Fe, NM, USA, 2014.
24. Sanchez, J. P., and Colombo, C. "Impact Hazard Protection Efficiency by a Small Kinetic Impactor," *Journal of Spacecraft and Rockets* Vol. 50, No. 2, 2013, pp. 380-393. doi: 10.2514/1.A32304